NANO LETTERS

pubs.acs.org/NanoLett

Plasmonic Structured Illumination Microscopy

Feifei Wei and Zhaowei Liu*

Department of Electrical and Computer Engineering, University of California, San Diego, La Jolla, California 92093-0407

ABSTRACT We propose a super resolution imaging technique called plasmonic structured illumination microscopy (PSIM), which combines the structured illumination microscopy technique with the tunable surface plasmon interference. Because of the high-resolution enabled by using surface plasmon interference as an illumination source, PSIM possesses higher image resolving power compared with conventional structured illumination microscopy. To demonstrate the technique, we present two specific types of plasmonic structure designs for PSIM. The final images from the simulations show 3-fold and 4-fold resolution improvement compared with conventional epi-fluorescence microscopy.

KEYWORDS Super resolution imaging, surface plasmons, structured illumination microscopy

Optical microscopy is an essential imaging technique in biology because of its ability to image living cells with negligible perturbations. However, the spatial resolution of a conventional lens-based optical microscope is fundamentally limited to $\sim\lambda/2\mathrm{NA}$, where λ is the wavelength of the light used and NA is the numerical aperture of the objective. This limits the resolution of an optical microscope image to about 200 nm for visible light; details smaller than that cannot be resolved. Since more and more biological studies require sub-100 nm or even molecular scale resolution, improving the resolution of optical microscopes to such scales will enable researchers to perform experiments using visible light without resorting to high-energy probes such as X-ray or electrons.

Within the last two decades, various techniques that can achieve subdiffraction limited resolution have been proposed and experimentally demonstrated, for example, near-field scanning optical microscopy (NSOM),[1−3] stimulated emission depletion microscopy (STED),[4,5] single molecular localization techniques,[6,7] structured illumination microscopy (SIM),[8−13] the far-field superlens (FSL),[14−16] the hyperlens,[17−19] and most recently the metamaterial immersion lens (MIL)[20] and plasmonic dark-field microscopy (PDF).[21] Despite their great successes in super resolution, these techniques still have various limitations.

Among the high-resolution imaging techniques, SIM is a method of special interest. It is suitable for in vivo biological imaging applications because it utilizes visible light (low-energy photon) and it is a highly parallelized scanning technique, which can potentially achieve high-imaging speed. SIM with a resolution of about twice the diffraction limit has already been experimentally demonstrated and used to acquire 3D multicolor high-resolution images of the nucleus of mammalian cells.[8−11] In conventional epi-fluorescence microscopy, only information with spatial frequencies that reside within the passband of the optical transfer function (OTF) of the objective can be detected. The OTF corresponds to a circular region of radius f_{cutoff} around the origin in Fourier space (the gray circle in Figure 1d), where f_{cutoff} defines the maximum resolvable spatial frequency. For conventional epi-fluorescence microscopes, f_{cutoff} is $\sim 2\mathrm{NA}/\lambda$. SIM utilizes the so-called "Moiré effect" to couple some of the high spatial frequency information from outside of the detectable region to inside the region to improve the resolution. For example, when an object with spatial frequency f (Figure 1a) overlaps with an illumination pattern with spatial frequency f_1 (Figure 1b), a Moiré fringe with spatial frequency $f - f_1$ (Figure 1c) is generated. If $f - f_1 < f_{\mathrm{cutoff}}$, the spatial frequency f can be detected by a microscope. The observed Moiré fringe image contains the contribution of the three components in Fourier space (represented by the red circles and the gray circle in Figure 1d) due to the spatial frequency mixing introduced by the structured illumination. To obtain a faithful high-resolution image, the three components in Fourier space need to be solved and moved back to their original positions. Therefore, multiple images with different illumination phases should be recorded and used to reconstruct the final high-resolution image through a numerical algorithm.[8−11,22] The saturated structured illumination microscopy (SSIM), proposed by Heintzmann[12] and experimentally demonstrated by Gustafsson,[13] can achieve even higher resolution compared to SIM by utilizing the nonlinear dependence of the fluorescence emission rate on the illumination intensity. The SSIM, however, has to cope with additional limitations such as fluorescence bleaching by strong illumination light intensity and slower imaging speed compared with SIM.

In SIM, $f_1 + f_{\mathrm{cutoff}}$ defines the largest spatial frequency that can be coupled into the passband of the OTF. The resolution improvement, $(f_1 + f_{\mathrm{cutoff}})/f_{\mathrm{cutoff}}$, is limited by the ratio f_1/f_{cutoff}. If we use the same objective for illumination and detection,

* To whom correspondence should be addressed. E-mail: zhaowei@ece.ucsd.edu.
Received for review: 03/29/2010
Published on Web: 05/27/2010

DOI: 10.1021/nl1011068 | *Nano Lett.* **2010,** *10,* 2531–2536

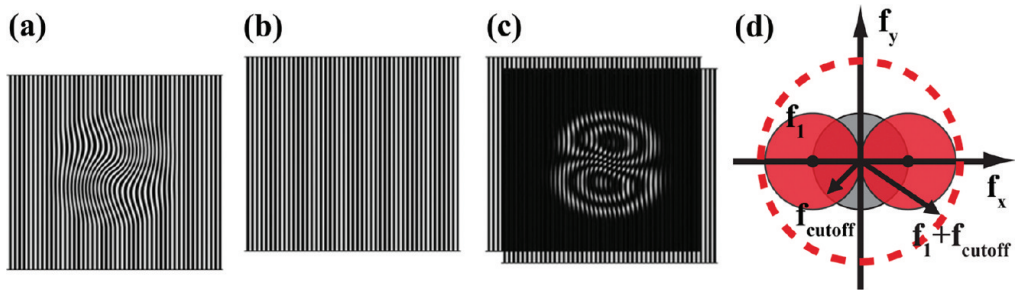

FIGURE 1. Concept of resolution enhancement in SIM. (a) An example object with small features; (b) a structured illumination pattern; (c) Moiré fringes formed by superposing structured illumination pattern (b) with object (a); (d) Fourier space representation of the SIM. The gray circle with radius f_{cutoff} corresponds to the accessible area of epi-fluorescence microscopes; the area between the red-dotted circle and gray circle represents the high-spatial frequency information that can be coupled into the detectable region through structured illumination. The shift in k space is determined by the spatial frequency of the illumination pattern f_1.

the spatial frequency shift f_1 ~2NA/$\lambda_{excitation}$ and the cutoff frequency f_{cutoff} ~2NA/$\lambda_{emission}$ are all determined by the NA of the objective. Considering $\lambda_{excitation}$ and $\lambda_{emission}$ are close for most cases, f_1 usually is close to f_{cutoff}. Therefore, the resolution for SIM ($1/(f_1 + f_{cutoff})$) is about $\lambda_{emission}/4NA$, roughly 2 times improvement compared with conventional epi-fluorescence microscopy.[9,11] To achieve a higher resolution improvement, illumination patterns with spatial frequencies larger than f_{cutoff} are needed. Besides light, surface plasmons (SPs) can also form interference patterns when multiple SP waves overlap.[23−25] Because the magnitude of the SP wavevector $|\mathbf{k}_{sp}|$ is typically much larger than that of the corresponding excitation light, the SP interference patterns possess much higher spatial frequency than any possible fringes formed by light with the same frequency. In addition, the spatial frequency of SP interference is not limited by the NA of the objective. Therefore SP interference is a good candidate to serve as the structured illumination pattern to further improve the resolution of SIM.

Here, we propose a new high-resolution optical imaging technique, called plasmonic structured illumination microscopy (PSIM), which combines the SP interference with SIM to achieve subdiffraction limited resolution without significantly decreasing the frame rate or utilizing the saturated fluorescence effect. Surface plasmons (SPs), also known as surface plasmon polaritons (SPPs), are electromagnetic waves formed by collective oscillations of electrons at a metal/dielectric interface.[26] The fundamental properties of SPs have been extensively studied since the 1970s and widely applied thereafter in many fields.[27−31] Recently, because of the significant advancement in nanoscale fabrication techniques, various fascinating applications of SPs have been experimentally demonstrated, including subdiffraction limited imaging,[14−21] subwavelength waveguide,[32,33] plasmonic lithography,[23−25] and optical negative refraction.[34] In this paper, we will first describe the physical principles of PSIM in detail and then numerically demonstrate its resolution improvement through two types of plasmonic structure designs. In the end, we will discuss both the advantages and disadvantages of this technique.

SPs possess a higher wave vector compared to the excitation photon. Figure 2 shows two typical dispersion curves for SPs (green curve and blue curves). The green curve corresponds to the dispersion relationship of SP modes at the semi-infinite-metal/dielectric interface, described as $|\mathbf{k}_{sp}| = |\mathbf{k}_{photon}|[(\varepsilon_m\varepsilon_d/(\varepsilon_m + \varepsilon_d)]^{1/2}$,[22] where $|\mathbf{k}_{photon}|$ and $|\mathbf{k}_{sp}|$ are the magnitude of the wave vectors of the excitation light in vacuum and of the SP, and ε_m and ε_d are the permittivity of the metal and dielectric, respectively. Since the dispersion curves of SPs always lie on the right side to that of the photon (red line in Figure 2), $|\mathbf{k}_{sp}|$ is always larger than the corresponding $|\mathbf{k}_{photon}|$. The ratio $|\mathbf{k}_{sp}|/|\mathbf{k}_{photon}|$ can be tuned by adjusting the frequency of the excitation light, the refractive index of the surrounding dielectric, or the thickness of the metal film.[23−25] For instance, as the frequency of the excitation light approaches the SP's resonant frequency, $|\mathbf{k}_{sp}|/|\mathbf{k}_{photon}|$ becomes extremely large (see Figure 2). For excitation light with a specific frequency, the ratio increases if the refractive index of the dielectric is increased. If both excitation light and surrounding media are fixed, the SP modes can also be adjusted by changing the thickness of the metal film. The typical SP dispersion relationship on a thin-metal-film/dielectric interface is presented as blue curves in Figure 2. All these SP modes possess higher wave vectors than that of the light. Furthermore, the different modes can be excited individually or simultaneously to form high-resolution interference patterns that can be used in PSIM.[35]

SPs can be excited by light as long as the momentum differences with the photons are compensated by coupling elements such as grating, edges, or slits.[23−25] Edges or slits are able to couple broadband light into SPs because their Fourier transforms contain broadband $\mathbf{k}$ vectors. Therefore, we use edges and slits to excite SPs in our simulations. If two counter propagating SP waves with wavelength λ_{sp} overlap, a uniform interference pattern with period equal to $\lambda_{sp}/2$ is formed.[23−25] To proceed with the image reconstruction, the phase of the illumination pattern needs to be changed multiple times during the image acquisition process.[8−13,22] For SP interference, the phase of the pattern can be changed by tuning the incident angle θ of the excitation

DOI: 10.1021/nl1011068 | *Nano Lett.* **2010,** *10,* 2531–2536

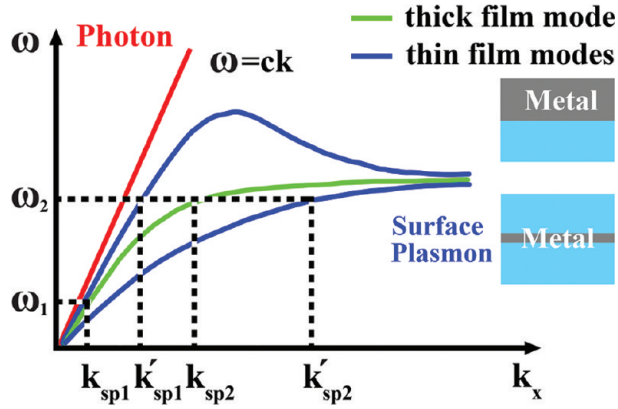

FIGURE 2. Typical dispersion curves of SPs on a semi-infinite-metal/dielectric interface and a thin-metal-film/dielectric interface.

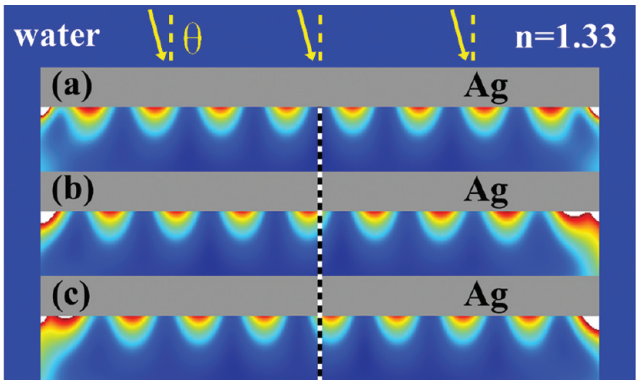

FIGURE 3. Numerical demonstration of the lateral shift of the SP interference pattern formed by the 563 nm excitation light with different incident angles. The simulation structure consists of a 1700 nm wide and 100 nm thick silver (Ag, gray area) stripe surrounded by water (blue area, $n = 1.33$). (a−c) The time-averaged electrical energy density distribution of the SP interference pattern with incident angle equal to 0, 4.6, and 8.0°, respectively. The three interference patterns show 120° mutual phase difference along the lateral direction.

light.[36] Under different incident angles, the light incident on the two adjacent edges or slits possesses a phase difference $\phi(\theta)$; this difference translates to the SPs also having a phase difference and thus changes the phase of the interference patterns. The simulation results in Figure 3 clearly show that the SP interference pattern shifts laterally with various incident angles.

In the following, we present two specific plasmonic designs, thick-metal-film/dielectric and thin-metal-film/dielectric structures, to serve as examples for PSIM demonstration and a guide for future development. The final reconstructed images are also provided to demonstrate the imaging performance of each design.

The structures of the two designs both consist of a layer of silver (Ag) film as the metal film and water as the surrounding dielectric. Ag is chosen as the supporting material because the SP frequency on Ag/dielectric interface covers the entire visible spectrum with relatively little loss. Water is used as the surrounding dielectric because many

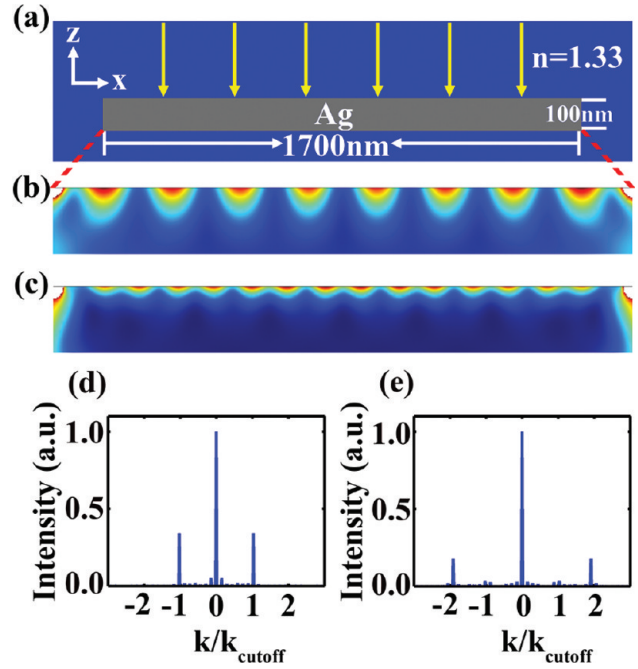

FIGURE 4. Numerical demonstrations of the SP interference at thick film/dielectric interface. (a) Structure configuration; (b,c) time-averaged electric energy density distribution excited by 563 and 390 nm light; (d,e) Fourier transform of (b,c) respectively.

biological samples are in an aqueous environment. In the SP interference simulation, the permittivity of Ag and Cr at different excitation frequencies was calculated by interpolating data from refs 37 and 38.

Specifically, for the thick-metal-film/dielectric structure, the thickness of the Ag film was chosen to be 100 nm so that it is thick enough to be treated as a semi-infinite interface. Excitation light with wavelengths of 390 and 563 nm were used to excite SP interference patterns. We assumed the fluorescent objects (for example quantum dots) absorb light at these excitation wavelengths and emit light at 580 nm. The fluorescent signal is detected by an objective with NA = 1.4. The distributions of the time-averaged electric energy density under the two illumination lights are shown in Figure 4b,c. The Fourier transforms of the illumination patterns, measured 20 nm under the Ag film, reveal peaks around $1k_{cutoff}$ and $2k_{cutoff}$, which is consistent with the calculated value from the analytical equation $|2\mathbf{k}_{sp1}|$ and $|2\mathbf{k}_{sp2}|$.

In the imaging performance simulations, SP interference patterns serve as the structured illumination patterns to illuminate a fluorescent object. For each orientation of illumination, a sequence of three images taken under illumination with different phases 0, 90, and 180° were used to solve the zeroth, ±first order components (gray and red circles in Figure 1d in Fourier space). The orientation of the illumination pattern is then rotated three times with a step of 45° in the $x-y$ plane to cover more areas in the Fourier space, yielding a total of 12 intermediate images for each final high-resolution image. The numerical algorithm of

DOI: 10.1021/nl1011068 | Nano Lett. 2010, 10, 2531–2536

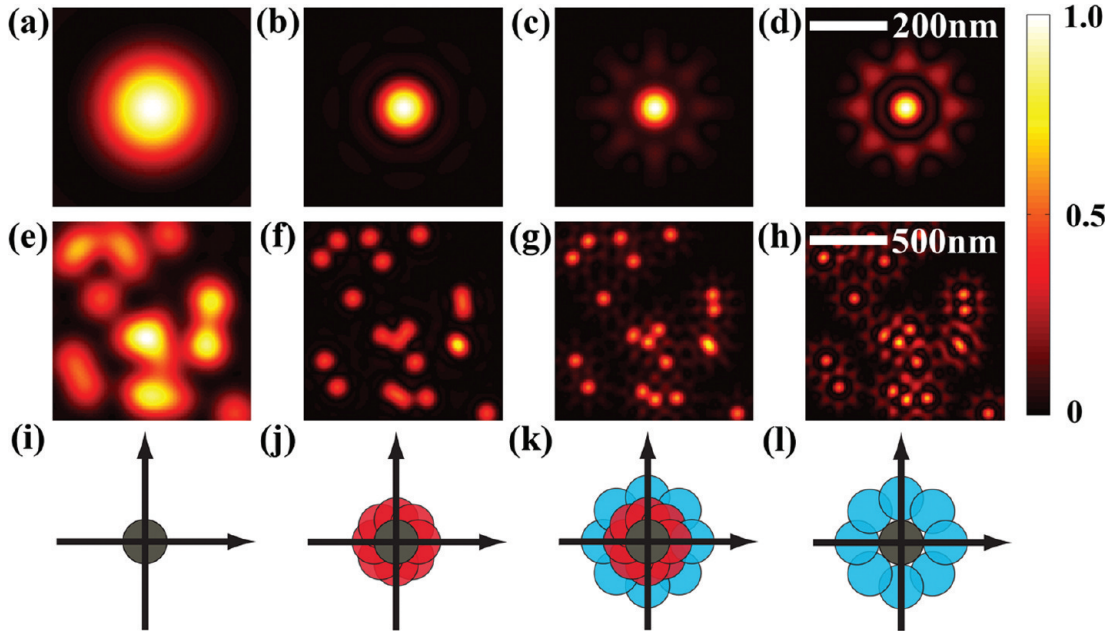

FIGURE 5. Point spread function of (a) conventional epi-fluorescence microscopy. (b) PSIM using 563 nm excitation light. (c) PSIM using 390 nm excitation light. (d) PSIM using both 563 and 390 nm excitation light. (e−h) Imaging performance demonstration for the case (a−d). Notice the scale bar difference between (a−d) and (e−h). (i−l) Corresponding k space representations. The gray circle represents the low-spatial frequency information that can be acquired through the epi-fluorescence microscope; the red and blue circles represent the high-spatial frequency information that can be coupled into the passband of the OTF through SP interference illumination excited by 563 and 390 nm light, respectively.

reconstructing high-resolution image from intermediate images is the same as that of SIM.[8−13,22] In the simulation, a 4 nm quantum dot (emission wavelength 580 nm) is used to acquire the point spread function (PSF). The full width half-maximum (FWHM) of the PSF shown in Figure 5a,c are about 214 and 74 nm respectively. The comparison between the PSF of conventional epi-fluorescence microscopy (Figure 5a) and that of PSIM (Figure 5b−d) shows an ∼3 times resolution improvement, which is better than the typical 2-fold improvement in SIM.[9,11] The simulation is also repeated for an object formed by randomly positioned 10 nm quantum dots (emission wavelength 580 nm) to further illustrate the imaging performance. Compared with the conventional epi-fluorescence microscopy image (Figure 5e), the reconstructed PSIM image sourced from 563 nm excitation light (Figure 5f), from 390 nm light (Figure 5h), and from the combination of the two (Figure 5g) all show drastic resolution improvements. Such improvement is also obvious from the coverage in the Fourier space representations (Figure 5i−l). The resolutions are about the same for Figure 5 panels g and h because the radii of the covered area in Fourier space are almost the same. However, the process of getting images (d,h) is twice as fast as that of getting images (c,g) because SP interference patterns with only one spatial frequency are used as the illumination source. Moreover, in principle, the artifacts in (d,h) can be removed by numerical processes.[9,11,13,39]

Since SP modes on thin-metal-film/dielectric interfaces possess even larger $\mathbf{k}$ vector compared with that on semi-infinite-metal/dielectric interface, we also designed a thin-metal-film/dielectric structure for PSIM. As shown in the structure of a unit cell (Figure 6a), an optimized Cr structure is used to excite the SP modes in the Ag thin film with relatively good efficiencies. When two modes (Figure 1 blue lines) are excited at the same time on the thin-metal-film/dielectric interface, the counter-propagating SP waves excited from two adjacent slits can form an interference pattern containing multiple spatial frequencies.[35] The thickness of the Ag film chosen is determined by the SP modes needed. In general, the larger the SP mode needed, the thinner the metal film. In this particular design, the thickness of the Ag film is 17 nm. Excitation light (442 nm) and fluorescent particles with 508 nm emission wavelength were used in the simulation. The NA is set to 0.85 so that a dry objective lens can be used for this design. The time-averaged electric energy density distribution measured 20 nm under the Ag film (Figure 6a) shows the multimode interference pattern. The corresponding Fourier Transform (Figure 6b) has peaks around $1k_{cutoff}$, $2k_{cutoff}$, and $3k_{cutoff}$, which is consistent with the first three peaks of the calculated values from the interference between the two SP modes ($|\mathbf{k'}_{sp2}| - |\mathbf{k'}_{sp1}|$, $2|\mathbf{k'}_{sp1}|$, $|\mathbf{k'}_{sp2}| + |\mathbf{k'}_{sp1}|$). The intensity of the fourth peak is so weak for this specific design that its contribution can be reasonably ignored. Using the same method as thick film simulations, we conducted the PSF simulation and imaging performance simulation for thin film structure. The conventional epi-fluorescence microscopy image and reconstructed images of an object formed by randomly positioned

DOI: 10.1021/nl1011068 | *Nano Lett.* **2010,** *10,* 2531–2536

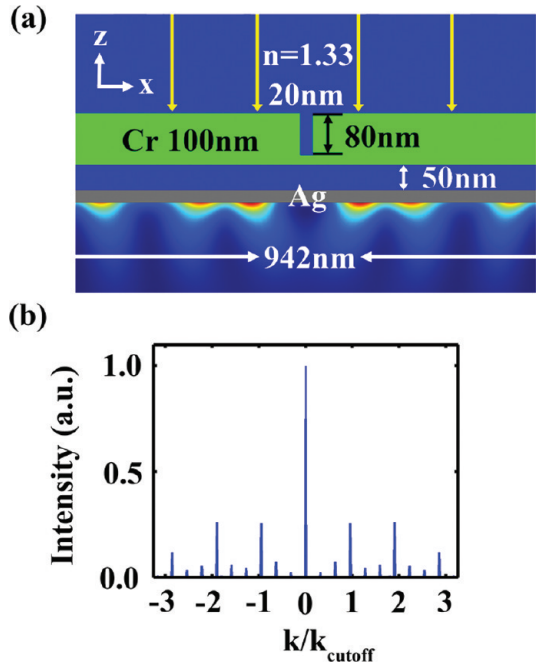

FIGURE 6. (a) Structure and SP interference pattern (time-averaged electric energy density distribution) excited by 442 nm light; (b) Fourier transform of interference pattern measured 20 nm under Ag film.

10 nm fluorescent particles are presented in Figure 7. The FWHM of PSF that corresponds to Figure 7h is about 76 nm, which corresponds to an ~4 times resolution improvement compared with the conventional epi-fluorecence microscopy.

One assumption we made in imaging simulations is that the fluorescence signal is proportional to the SP intensity. The second assumption is that the change of the SP interference patterns is negligible with the presence of the fluorescence object, because the existence of the fluorescence dye will not considerably alter the SP propagation length in experiment.[40] Moreover, we want to emphasize that the detected light is not the SP interference patterns but the emission light from fluorescent particles or quantum dots. Therefore, although the SP interference patterns only exist at the near field of the metallic surface, we can still record the image from far field. The two designs described above serve as examples to demonstrate the imaging principles and performance of PSIM. On the basis of the simulation results, we can conclude that PSIM can achieve subdiffraction limit resolution. Moreover, the wave vector of SP mode is adjustable by changing the structure. Depending on the applications, various parameters such as the excitation wavelength, refractive index of the surrounding media, material, as well as structures can be adjusted in order to get better improvement in terms of resolution, speed, or both. While we only showed 1D SP interference pattern in our numerical simulations, it is possible to acquire 2D SP interference pattern through proper designs.[24,25] There is no limitation on the imaging size of the PSIM if a periodic plasmonic structure is utilized, although the period of the structure should be limited by the SP propagation length.

One of the advantages of PSIM is that the resolution does not solely depend on the NA of the optical microscope, as with SIM. The resolution of SIM can be written as $\lambda_{emission}/[2NA + 2NA(\lambda_{emission}/\lambda_{excitation})]$, which is approximately $\lambda_{emission}/4NA$ when $\lambda_{emission}/\lambda_{excitation}$ is about 1, while the resolution of PSIM is $\lambda_{emission}/(2NA + 2NA_{effective})$, in which $NA_{effective}$ is $\lambda_{emission}/\lambda_{sp}$. Since $\lambda_{emission}/\lambda_{sp}$ is independent of objectives and usually larger than a possible NA provided by common objectives, PSIM can achieve higher resolution than SIM even with small NA objectives. Also, PSIM has higher resolution improvement compared with a pure dielectric structure. Since the dispersion curve of SPs lie on the right side of that of the photons in the same media, metal/dielectric structures can always generate interference patterns with larger spatial frequency compared to a dielectric structure. Moreover, PSIM can selectively excite fluorescent objects in a thin region close to the metal surface because the SP exponentially decays along the z direction. Therefore, fluorescent

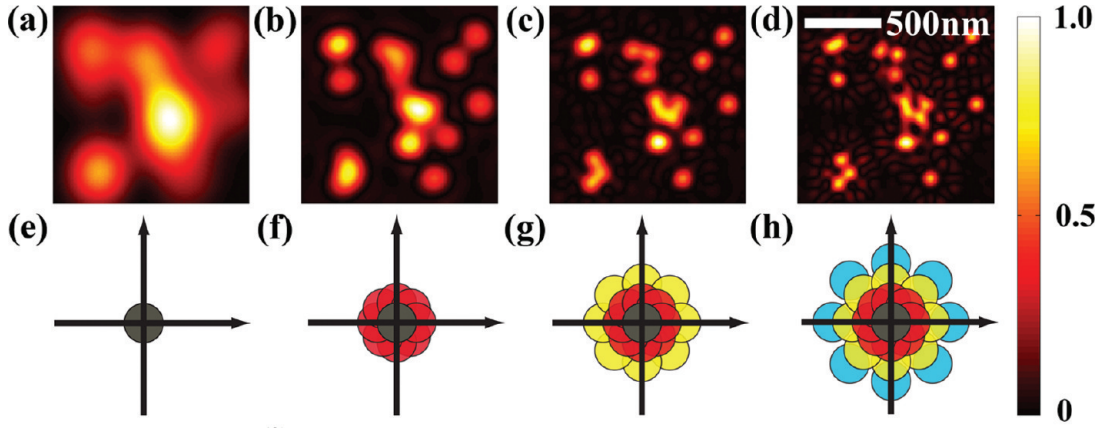

FIGURE 7. PSIM imaging ability demonstration. (a) Conventional epi-fluorescence microscope image; (b−d) Reconstructed images; (e−h) Corresponding k space representations. Different colors represents the information obtained from different orders of the illumination patterns.

DOI: 10.1021/nl1011068 | *Nano Lett.* **2010,** *10,* 2531--2536

particles that are far from the interface will not contribute to the strong background as in the case of conventional epifluorescence microscopy. In general, the z direction imaging depth depends on the resolution improvement along the $x-y$ directions, and usually decreases as the $x-y$ resolution increases.[26] If the imaging region of interest is only several tens of nanometers away from the interface, PSIM is a good imaging tool to use. Multicolor imaging is possible since SP modes with different frequencies can be generated by excitation light with the corresponding frequencies on a properly designed metallic structure. PSIM itself does not require a high-power laser, but it can also be combined with the nonlinear dependence of the emission rate on the illumination intensity. Similarly to SSIM, through utilizing higher harmonic peaks, saturated PSIM can achieve even greater resolution improvement.

Besides the various advantages mentioned above, this technique also has its limitations. PSIM is intrinsically a 2D imaging technique that can only form a high-resolution image of objects close to the metal surface. Although a spacer layer between the object and the metal film can reduce the quenching effect,[41,42] the fluorescence efficiency is less in PSIM than in conventional SIM. Moreover, complicated designs might be needed for higher resolution improvement. Since the decay length along both $x-y$ and z directions gets shorter as the wave vector of the SP increases, researchers may need to find a balance when doing actual designs.

In conclusion, a new super-resolution imaging technique, plasmonic structured illumination microscopy (PSIM) is numerically demonstrated. Simulation results have shown that a resolution improvement larger than that of SIM can be achieved without utilizing nonlinear dependence of the fluorescence emission rate on the illumination intensity. The reconstructed images using two plasmonic designs show 3-fold and 4-fold resolution improvement compared to epifluorescence microscopy. The PSIM may have important applications in the field of high-resolution biomedical imaging.

Acknowledgment. We thank A. A. Schfagans, R. Aguinaldo and G. C. So for their useful discussions. This research is partially supported by NSF-ECCS under Grant 0969405.

REFERENCES AND NOTES

(1) Ash, E. A.; Nicholls, G. *Nature* **1972**, *237*, 510–512.
(2) Lewis, A.; Isaacson, M.; Harootunian, A.; Murray, A. *Ultramicroscopy* **1984**, *13*, 227.
(3) Pohl, D. W.; Denk, W.; Lanz, M. *Appl. Phys. Lett.* **1984**, *44*, 651.
(4) Hell, S. W.; Wichmann, J. *Opt. Lett.* **1994**, *19*, 780–782.
(5) Dyba, M.; Hell, S. W. *Phys. Rev. Lett.* **2002**, *88*, 163901.
(6) Rust, M. J.; Bates, M.; Zhuang, X. *Nat. Methods* **2006**, *3*, 793–796.
(7) Betzig, E.; Patterson, G. H.; Sougrat, R.; Lindwasser, O. W.; Olenych, S.; Bonifacino, J. S.; Davidson, M. W.; Lippincott-Schwartz, J.; Hess, H. F. *Science* **2006**, *313*, 1642–1645.
(8) Heintzmann, R.; Cremer, C. *Proc. SPIE* **1998**, *3568*, 185–195.
(9) Gustafsson, M. G. L. *J. Microsc.* **2000**, *198*, 82–87.
(10) Frohn, J. T.; Knapp, H. F.; Stemmer, A. *Proc. Natl. Acad. Sci. U.S.A.* **2000**, *97*, 7232–7236.
(11) Schermelleh, L.; Carlton, P. M.; Haase, S.; Shao, L.; Winoto, L.; Kner, P.; Burke, B.; Cardoso, M. C.; Agard, D. A.; Gustafsson, M. G. L.; Leonhardt, H.; Sedat, J. W. *Science* **2008**, *320*, 1332–1336.
(12) Heintzmann, R.; Jovin, T. M.; Cremer, C. *J. Opt. Soc. Am. A* **2002**, *19* (8), 1599–1609.
(13) Gustafsson, M. G. L. *Proc. Natl. Acad. Sci. U.S.A.* **2005**, *102* (37), 13081–13086.
(14) Durant, S.; Liu, Z.; Steele, J. M.; Zhang, X. *J. Opt. Soc. Am. B* **2006**, *23*, 2383–2392.
(15) Liu, Z.; Durant, S.; Lee, H.; Pikus, Y.; Fang, N.; Xiong, Y.; Sun, C.; Zhang, X. *Nano Lett.* **2007**, *7* (2), 403–408.
(16) Xiong, Y.; Liu, Z.; Sun, C.; Zhang, X. *Nano Lett.* **2007**, *7* (11), 3360–3365.
(17) Salandrino, A.; Engheta, N. *Phys. Rev. B* **2006**, *74*, No. 075103.
(18) Jacob, Z.; Alekseyev, L. V.; Narimanov, E. *Opt. Express* **2006**, *14* (18), 8247–8256.
(19) Liu, Z.; Lee, H.; Xiong, Y.; Sun, C.; Zhang, X. *Science* **2007**, *315*, 1686.
(20) Ma, C.; Liu, Z. *Opt. Express* **2010**, *18*, 4838.
(21) Hu, H.; Ma, C.; Liu, Z. *Appl. Phys. Lett.* **2010**, *96*, 113107.
(22) Krishnamurthi, V.; Bailey, B.; Lanni, F. *SPIE* **1996**, *2655*, 18–25.
(23) Luo, X.; Ishihara, T. *Appl. Phys. Lett.* **2004**, *84* (23), 4780–4782.
(24) Liu, Z.; Wei, Q.; Zhang, X. *Nano Lett.* **2005**, *5*, 957–961.
(25) Xiong, Y.; Liu, Z.; Zhang, X. *Appl. Phys. Lett.* **2008**, *93*, 111116.
(26) Raether, H. *Surface Plasmons on Smooth and Rough Surfaces and on Gratings*; Springer-Verlag: Berlin Heidelberg, Germany, 1988.
(27) Pockrand, I.; Swalen, J. D.; Gordon, J. G.; Philpott, M. R. *Surf. Sci.* **1978**, *74*, 237–244.
(28) Nylander, C.; Liedberg, B.; Lind, T. *Sens. Actuators* **1982**, *3*, 79–88.
(29) Jeanmaire, D. L.; Van Duyne, R. P. *J. Electroanal. Chem.* **1977**, *84*, 1–20.
(30) Albrecht, M. G.; Creighton, J. A. *J. Am. Chem. Soc.* **1977**, *99* (15), 5215.
(31) Moskovits, M. *Rev. Mod. Phys.* **1985**, *57*, 783.
(32) Pile, D. F. P.; Gramotnev, D. K. *Opt. Lett.* **2005**, *30*, 1186–1188.
(33) Bozhevolnyi, S. I.; Volkov, V. S.; Devaux, E.; Laluet, J.; Ebbesen, T. W. *Nature* **2006**, *440*, 508–511.
(34) Yao, J.; Liu, Z.; Liu, Y.; Wang, Y.; Sun, C.; Bartal, G.; Zhang, X. *Science* **2008**, *321*, 930.
(35) Yao, J.; Liu, Y.; Liu, Z.; Sun, C.; Zhang, X. *Proc. of SPIE* **2006**, 6323.
(36) Liu, Z.; Steele, J. M.; Lee, H.; Zhang, X. *Appl. Phys. Lett.* **2006**, *88*, 171108.
(37) Weber, M. J. *Handbook of Optical Materials*; CRC Press: Boca Raton, FL, 2003.
(38) Johnson, P. B.; Christy, R. W. *Phys. Rev. B,* **1972**, *6*, 4370–4379.
(39) Richardson, W. H. *J. Opt. Soc. Am.* **1972**, *62* (1), 55–59.
(40) Ditlbacher, H.; Krenn, J. R.; Schider, G.; Leitner, A.; Aussenegg, F. R. *Appl. Phys. Lett.* **2002**, *81*, 1762–1764.
(41) Weber, W. H.; Eagen, C. F. *Opt. Lett.* **1979**, *4*, 236–238.
(42) Ditlbacher, H.; Krenn, J. R.; Felidj, N.; Lamprecht, B.; Schider, G.; Salerno, M.; Leitner, A.; Aussenegg, F. R. *Appl. Phys. Lett.* **2002**, *80*, 404–406.

DOI: 10.1021/nl1011068 | *Nano Lett.* **2010,** *10,* 2531–2536